IRANIAN

JOURNAL

OF

VETERINARY

RESEARCH

Original Article

A neuroanatomical study of the feline brain using MRI and mulligan staining: functional and pathological considerations

Díaz Martínez, E.[1]; Ayala Florenciano, M. D.[1]; Arencibia Espinosa, A.[2]; Soler Laguía, M.[3]; Kilroy, D.[4]; Martínez Gomariz, F.[1] and Ramírez Zarzosa, G.[1*]

[1]Department of Anatomy and Compared Pathological Anatomy, Veterinary Faculty, Campus de Espinardo, University of Murcia, 30100, Murcia, Spain; [2]Department of Morphology, Veterinary Faculty, University of Las Palmas de Gran Canaria, Trasmontaña, Arucas, 35413, Las Palmas, Spain; [3]Department of Medicine and Surgery, Veterinary Faculty, Campus de Espinardo, University of Murcia, 30100, Murcia, Spain; [4]Division of Veterinary Science Centre, University College Dublin, School of Veterinary Medicine, University of Dublin, Belfield, Dublin 4, Ireland

[*]*Correspondence: G. Ramírez Zarzosa, Department of Anatomy and Compared Pathological Anatomy, Veterinary Faculty, Campus de Espinardo, University of Murcia, 30100, Murcia, Spain. E-mail: grzar@um.es*

Abstract

Background: Despite multiple studies describing accurate diagnoses using advanced neuroimaging techniques, low and mid-field magnetic resonance imaging (MRI) are still the most frequent scanners in veterinary clinics. To date, these studies in cats do not show a clear distinction of nerve centres in MRI data. **Aims:** The objective of this study is to determine the efficacy of Mulligan histological staining as a tool in facilitating the location and identification of the main structures of the feline brain in MRI. This study aims to facilitate the interpretation of MRI obtained with these types of scanners. **Methods:** A total of 10 feline brains were used. One specimen was used for MRI (T2 sequence using a 1.5T scanner). The other 9 brains were sectioned and stained with the three Mulligan staining techniques (Mulligan, Le Masurier and Robert). **Results:** The uptake of stain by the grey matter in these sections allowed the determination of the location and the limits of these nervous structures within the brain. The histological location of these structures was correlated with the MRI scans, leading to the successful identification of many small, indistinct nuclei. **Conclusion:** Mulligan staining is proposed as a tool that facilitates the location of nerve structures in comparison with data from the most frequently-used MRI scanners in veterinary clinics.

Key words: Feline, MRI, Mulligan staining, Nervous nuclei, Neuroanatomy

Introduction

In neurology, the main diagnostic imaging technique is magnetic resonance imaging (MRI), producing images used to identify numerous structures of the brain. This imaging technique is widely used in advanced studies of the central nervous system (CNS) of experimental animals (Müllhaupt *et al*., 2015) as well as its daily use in the diagnosis of neurological pathologies of domestic animals. There are numerous MRI studies on visible alterations of the hippocampus in epileptic dogs and cats (Claßen *et al*., 2016). In addition, numerous brain structures have been identified in MRI atlases; however, due to a large number of structures within the brain, MRI image resolution does not allow for their clear differentiation (Mogicato *et al*., 2012; Gray-Edwards *et al*., 2014). Although MRI scanners are classified as low (0.4T) and high-field units (3T), nowadays ultra-high-field MRI equipment (11.4T) has been developed (Hespel and Cole, 2018). Moreover, several advanced neuroimaging techniques have been developed, which allow for highly detailed studies of the feline brain. The

anatomical distribution and connections of white matter can be further differentiated by diffusion spectrum imaging tractography from diffusion magnetic imaging (Das and Takahashi, 2018; Johnson *et al*., 2020). Similarly, the cytoarchitecture and electrophysiology of the feline brain has been studied by Stolzberg *et al*. (2017), but this was achieved using a 7T MRI scanner. However, the ultra-high-field MRI increases the cost and its use is limited to experimental and human pathology studies (Ghaznawi *et al*., 2018). Access to high magnetic field equipment (from 3T upwards) in veterinary clinics used to be quite rare (Przyborowska *et al*., 2017). For this reason, we have focused our study on low and high-field units of MRI equipment as these are more accessible to veterinary clinicians.

These continuous advances often discard old histological methods (Mulligan staining), which provide clear differentiation between the white and the grey matter in the brain (Mulligan, 1931). This staining initially was a unique technique, later developed to different methods leading to improved results (Mooncey and Sagoo, 2014). This staining technique is effective in

locating and identifying nervous nuclei. Many studies in humans show the efficacy of this staining technique in differentiating between white and grey matter (De Meneses *et al*., 2004). For example, some recent studies have been carried out in certain nervous nuclei, such as the nucleus accumbens (Oldoni *et al*., 2018) and the internal globus pallidus (lentiform nucleus) (Dos Santos *et al*., 2019). However, the absence of studies correlating stained encephalic sections (Mulligan) with MRI led to this research which helps in the interpretation of MRI by rescuing an almost forgotten technique, but one with considerable use in the study of CNS structures.

This study is presented as an MRI neuroanatomic atlas that aims to aid the veterinary clinician in the identification of the main nervous nuclei and nerve structures that are affected in common nerve pathologies. In this regard, Mulligan staining has allowed the accurate location of nerve structures by comparison with the most frequently-used MRI scanners in veterinary clinics.

Materials and Methods

Specimens used

Ten adult cats (2-3 years old, average weight 4 kg BW) obtained from the Public Health Service of Murcia were humanely euthanized for causes not related to this study. This experiment was supervised by the Ethics Commission of the University of Murcia (CEAA 305/2017).

The heads were trephined and the brains were extracted and fixed for two weeks in 10% formaldehyde solution. Only one brain was used for the MRI study. The other 9 specimens were sectioned in the three spatial planes and stained using Mulligan, Le Masurier and Robert techniques (Mulligan, 1931; LeMasurier, 1935; Barnard *et al*., 1949).

Magnetic resonance protocol

MRI data were acquired employing spin-echo T1 and T2-weighting sequences in sagittal, transverse, and dorsal planes. Only the T2-weighting is attached as it provided a greater differentiation than T1-weighting between nuclear structures and consequently has a greater diagnostic value. The MRI study was performed using a high-field MRI apparatus 1.5 Tesla (General Electric Sigma Excite, Schenectady, USA). For MRI, the brain was placed in a high-resolution wrist coil and arranged as if the animal were positioned in ventral recumbency on the MRI couch. The small size of the cat brain scanned on a human wrist coil caused distortion of the outer margins of the brain on MRI, but the nuclear structures remain unchanged. MRI was saved in DICOM format and analysed with a Radiant DICOM viewer.

Sequence parameters are presented in Table 1.

Mulligan staining

The Mulligan staining method was used for this study. Le Masurier and Robert techniques are variations of the Mulligan technique using different staining solutions and staining times as described by Mooncey

and Sagoo (2014).

Feline heads were cut in three spatial planes (0.5-0.6 cm thick) using an electric band saw. Head sections were fixed for seven days in 10% formaldehyde solution. Brain sections were removed and then stained using Mulligan staining. The protocol to prepare Mulligan solution is described in Table 2. The protocols of each staining technique are presented in Tables 3, 4, and 5.

All photographs were taken with Nikon® D-40 camera, on a black background, and the software used to make the photographic compositions was Adobe Photoshop® CS6.

Table 1: MRI sequence parameters

Parameters	SE T2-weighted
Repetition time (ms)	Sagittal: 440 Transverse: 1200 Dorsal: 500
Echo time (ms)	Sagittal: 15 Transverse: 22 Dorsal: 15
Inversion time (ms)	Sagittal: 0 Transverse: 0 Dorsal: 0
NEX	Sagittal: 1 Transverse: 1 Dorsal: 1
Slice thickness (mm)	Sagittal: 2 Transverse: 2 Dorsal: 2
Interslice gap (mm)	Sagittal: 2.2 Transverse: 2 Dorsal: 2
Field of view	Sagittal: 100 Transverse: 100 Dorsal: 100
Matrix dimensions (mm)	Sagittal: 256 × 192 Transverse: 192 × 192 Dorsal: 256 × 192

Table 2: Protocol of Mulligan solution

Mulligan solution	
Reagents	Temperature
40 g crystallized phenol	65°C
5 g copper sulphate	
1.25 ml hydrochloric acid 0.1M	
Add distilled water up to 1 L and mix	

Table 3: Protocol of Mulligan staining technique

Mulligan staining technique (purple)		
Solutions	Time	Temperature
Mulligan solution	4 min	66°C
Tap water	10 s	Cold
2% tannic acid in a 10% methanol solution	1 min	Room temperature
0.6% ferric ammonium sulfate solution	10-15 s	Room temperature
Tap water	1 h	Room temperature

Table 4: Protocol of Le Masurier staining technique

Le Masurier staining technique (blue)		
Solutions	Time	Temperature
Mulligan solution	2 min	60-65ºC
Tap water	1 min	Cold
2% ferric chloride solution	2 min	Room temperature
Tap water	5 min	Room temperature
1% potassium ferrocyanide solution	10-12 s	Room temperature
Tap water	2 min	Cold
Tap water	1 h	Room temperature

Table 5: Protocol of Robert staining technique

Robert staining technique (pink)		
Solutions	Time	Temperature
Mulligan solution	6 min	60-65ºC
Tap water	5 min	Cold
2% potassium ferrocyanide solution	10 s	Room temperature
Tap water	1 h	Room temperature

Anatomical study

All stained brain structures were identified based on a complete neuroanatomical bibliography. As it provides accurate information detailing the location of many nuclei in different planes Nickel *et al*. (1988) was the basis for the interpretation of most of the nuclear structures in stained sections. Sandoval (2000) also facilitated the nuclear interpretation. MRI were interpreted by extrapolation from the structures identified in stained sections, along with consultation of other studies of feline brain MRI such as Gray-Edwards *et al*. (2014) and Przyborowska *et al*. (2017).

Results

Anatomical description

Our results are shown in Figs. 1A-C, 2A-D to 7A-D, 8A-B, and 9. Figures 2A-D to 7A-D show a sequence of brain cross sections stained with the three Mulligan staining techniques, correlated with corresponding MRI.

Cerebellum

A clear distinction between the cerebellar white and grey matter was observed with Le Masurier staining technique and the well-known "tree of life" was visualized in great detail (Figs. 8A-B).

In the stained cross sections of the cerebellum, at the level of the caudal lobe of the cerebellum and the medulla oblongata, important nuclei were identified in the thickness of the white matter: the emboliform, globose and fastigial nuclei (Figs. 2A-D). All these nuclei were visualized in hyperintense areas in T2-weighted MRI (Fig. 2A).

Brain stem

In the thickness of the medulla oblongata, the vestibular and olivary nuclei, as well as the reticular formation were observed dyed in a transverse plane (Figs. 2A-D). The stained ceruleus nucleus was ventral to the cerebellum (Figs. 7A-D). These nuclear structures were difficult to locate in the T2-weighted MRI.

At the level of the midbrain, the mesencephalic aqueduct was surrounded by stained central grey matter

and it was visualized as a hyperintense area in T2-weighted images (Figs. 3A-D to 4A-D). At this level, the red nucleus appeared dyed, as well as the substantia nigra, which delimited the undyed pyramidal and corticopontine tracts. The reticular formation and the red nucleus were only seen as hyperintense areas in T2-weighted sequences. Due to its greater intensity, the substantia nigra could be located in T2-weighted images.
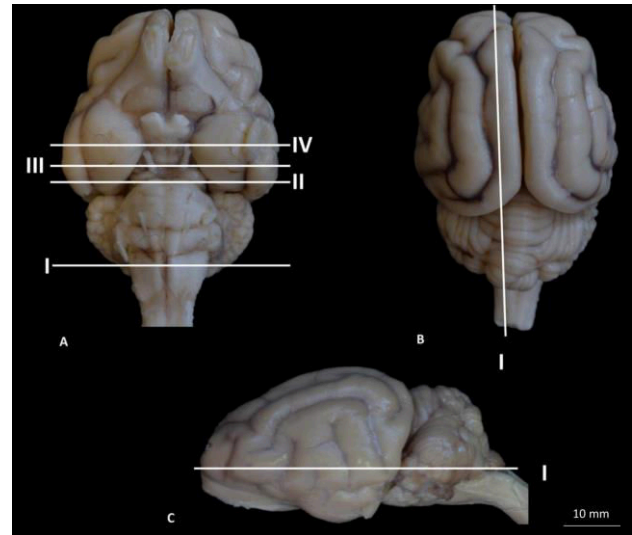

Fig. 1: Approximate level sections of the cat brain in ventral, dorsal, and lateral view. The lines represent the transversal, sagittal, and frontal location of each MR image and its corresponding staining at the same level. (**A**) Levels of cross sections in ventrodorsal direction, (**B**) Level of sagittal section, and (**C**) Level of frontal section
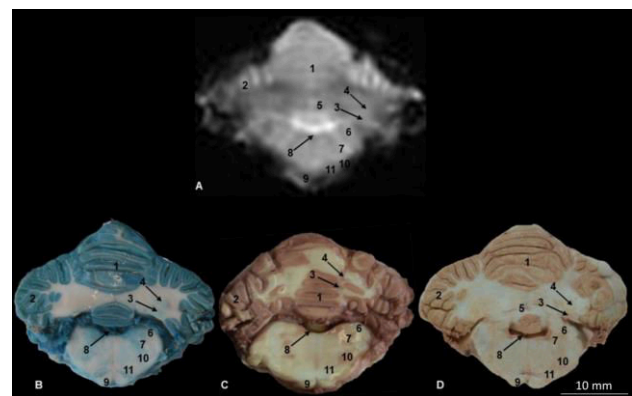

Fig. 2: Cross section at the approximate level of the caudal lobe of cerebellum and medulla oblongata of the cat brain. (**A**) T1-weighted MRI, (**B**) Mulligan staining (Le Masurier), (**C**) Mulligan staining (Mulligan), and (**D**) Mulligan staining (Robert). 1: Cerebellar vermis, 2: Cerebellar hemispheres, 3: Lateral interposed nucleus (emboliform nucleus), 4: Medial interposed nucleus (globose nucleus), 5: Roof nucleus (fastigial nucleus), 6: Cerebellar peduncles, 7: Vestibular nuclei, 8: Fourth ventricle, 9: Pyramidal tracts, 10: Tegmental pontine reticular nucleus, and 11: Olivary nuclei

Diencephalon

With its circular shape, the lateral geniculate nucleus was well defined on both sides of the thalamus (Figs.

5A-D to 7A-D, 8A-B, and 9). The medial geniculate body was stained with the Mulligan technique (Fig. 4C). None of these structures could be seen clearly in MRI. The thalamus appeared stained compactly and with great intensity, with the zona incerta and the subthalamic nucleus the most easily identified nuclei (Figs. 5A-D). The dorsal nuclei of the thalamus were also visualized in a coronal plane (Figs. 6A-D). In the MRI, the thalamus was identified as a hyperintense area, but its internal nuclei could not be identified.
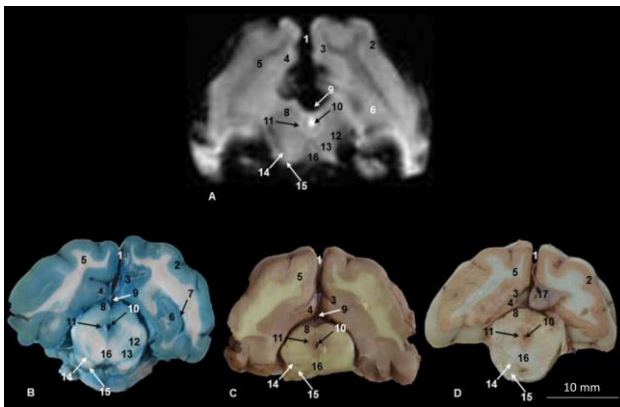

Fig. 3: Cross section at the approximate level of the mesencephalon and occipital lobe of the cerebral hemispheres of the cat. (**A**) T2-weighted MRI, (**B**) Mulligan staining (Le Masurier), (**C**) Mulligan staining (Mulligan), and (**D**) Mulligan staining (Robert). 1: Longitudinal fissure of the brain, 2: Suprasylvian sulcus, 3: Splenial sulcus, 4: Cingulate gyrus, 5: Optic radiation, 6: Hippocampus, 7: Lateral ventricle: temporal horn, 8: Rostral colliculus: grey matter, 9: Pineal recess, 10: Mesencephalic aqueduct, 11: Central grey matter, 12: Reticular formation, 13: Red nucleus, 14: Substantia nigra, 15: Cerebellar peduncle: pyramidal tract, 16: Interpeduncular nucleus, and 17: Pineal gland or epiphysis (displaced and sectioned)
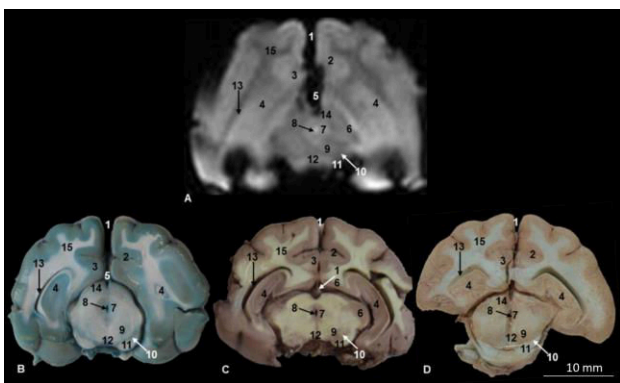

Fig. 4: Cross section at the approximate level of the mesencephalon and temporal lobe of the cerebral hemispheres of the cat. (**A**) T2-weighted MRI, (**B**) Mulligan staining (Le Masurier), (**C**) Mulligan staining (Mulligan), and (**D**) Mulligan staining (Robert). 1: Longitudinal fissure of the brain, 2: Splenial sulcus, 3: Cingulate gyrus, 4: Hippocampus, 5: Pineal recess, 6: Medial geniculate body, 7: Central grey matter, 8: Mesencephalic aqueduct, 9: Red nucleus, 10: Substantia nigra, 11: Cerebellar peduncle: pyramidal tract, 12: Interpeduncular nucleus, 13: Lateral ventricle: temporal horn, 14: Rostral colliculus: grey matter, 15: Optic radiation, and 16: Pineal gland or epiphysis

Telencephalon

The stained hippocampus was observed in transverse, coronal, and sagittal planes (Figs. 4A-D to 7A-D). In the T2-weighted sequence, it was identified as a
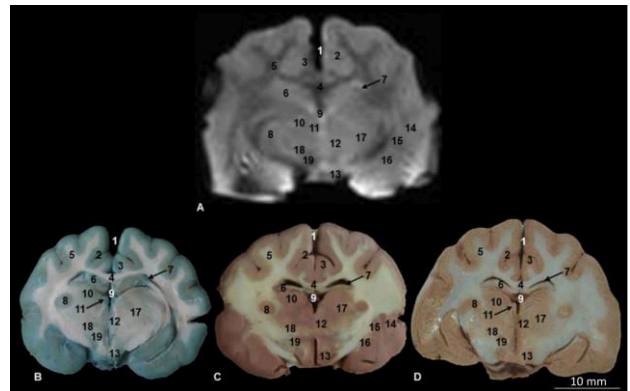

Fig. 5: Cross section at the approximate level of the thalamus and temporal cortex of the cerebral hemispheres of the cat. (**A**) T2-weighted MRI, (**B**) Mulligan staining (Le Masurier), (**C**) Mulligan staining (Mulligan), and (**D**) Mulligan staining (Robert). 1: Longitudinal fissure of the brain, 2: Splenial sulcus, 3: Cingulate gyrus, 4: Corpus callosum, 5: Acoustic radiation, 6: Hippocampus, 7: Lateral ventricle, 8: Lateral geniculate nucleus, 9: Pineal gland or epiphysis, 10: Rostral thalamic nuclei, 11: Habenular nuclei, 12: Paraventricular nuclei of the thalamus, 13: Mammillary body: mammillary nuclei, 14: Claustrum, 15: Lentiform nucleus: putamen, 16: Lentiform nucleus: globus pallidus, 17: Thalamus, 18: Zona incerta, and 19: Subthalamic nucleus
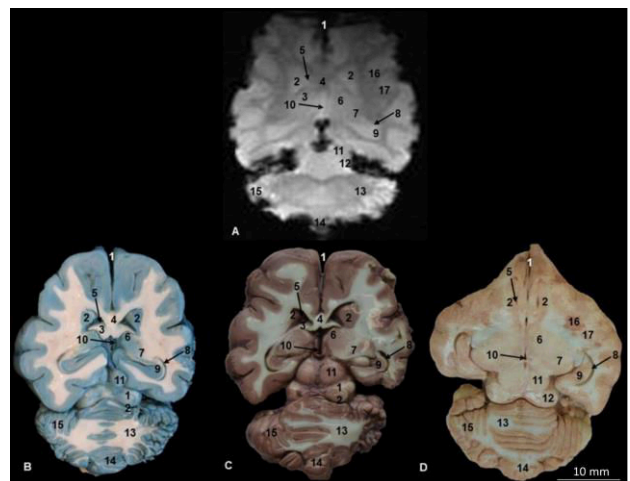

Fig. 6: Coronal section of the brain at the approximate level of the cerebellum, mesencephalon, and corpus striatum of the cerebral hemispheres. (**A**) T2-weighted MRI, (**B**) Mulligan staining (Le Masurier), (**C**) Mulligan staining (Mulligan), and (**D**) Mulligan staining (Robert). 1: Longitudinal fissure of the brain, 2: Caudate nucleus: head, 3: Corpus callosum: genu, 4: Rostral commissure, 5: Lateral ventricle: rostral horn, 6: Dorsal nuclei of thalamus, 7: Lateral geniculate body, 8: Lateral ventricle: temporal horn, 9: Hippocampus, 10: Third ventricle, 11: Mesencephalon: rostral colliculus, 12: Mesencephalon: caudal colliculus, 13: Cerebellum: white matter, 14: Cerebellum: vermis, 15: Cerebellum: grey matter, 16: Lentiform nucleus: globus pallidus, and 17: Lentiform nucleus: putamen
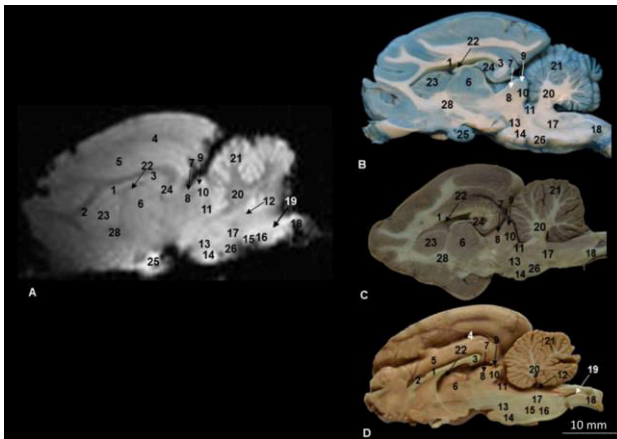
Fig. 7: Sagittal section of the cat brain. (**A**) T2-weighted MRI, (**B**) Mulligan staining (Le Masurier), (**C**) Mulligan staining (Mulligan), and (**D**) Mulligan staining (Robert). 1: Corpus callosum: body, 2: Corpus callosum: genu, 3: Corpus callosum: splenium, 4: Splenial sulcus, 5: Cingulate gyrus, 6: Thalamus: interthalamic adhesion or intermediate mass, 7: Rostral colliculus, 8: Grey stratum of the rostral colliculus, 9: Caudal colliculus, 10: Caudal colliculus nucleus, 11: Ceruleus nucleus, 12: Fourth ventricle, 13: Pons, 14: Pontine nuclei, 15: Olivary nuclei, 16: Arcuate nucleus, 17: Medulla oblongata, 18: Spinal cord, 19: Ependyma, 20: Cerebellum: medullary body, 21: Cerebellum: cerebellar cortex, 22: Lateral ventricle, 23: Caudate nucleus: head, 24: Hippocampus, 25: Hypophysis, 26: Trapezoid body, 27: Bulbar pyramid, and 28: Internal capsule
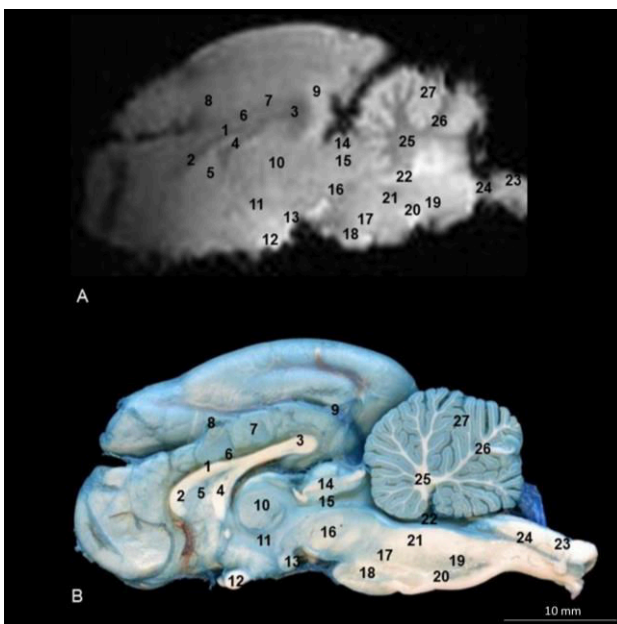

Fig. 8: Sagittal section of the cat brain. (**A**) T2-weighted MRI, and (**B**) Mulligan staining (Le Masurier). 1: Corpus callosum: body, 2: Corpus callosum: genu, 3: Corpus callosum: splenium, 4: Fornix, 5: Septum of the telencephalum, 6: Sulcus of corpus callosum, 7: Cingulate gyrus, 8: Splenial sulcus, 9: Calcarine sulcus, 10: Thalamus: interthalamic adhesion, 11: Third ventricle, 12: Optic chiasm, 13: Hypothalamus: mammillary body, 14: Mesencephalic tectum: colliculus, 15: Mesencephalic aqueduct, 16: Cerebral peduncle: tegmentum, 17: Pons, 18: Pontine nuclei, 19: Olivary nuclei, 20: Arcuate nucleus, 21: Medulla oblongata, 22: Fourth ventricle, 23: Spinal cord, 24: Ependyma, 25: Cerebellum: medullary body, 26: Cerebellum: white laminae, and 27: Cerebellum: cerebellar cortex
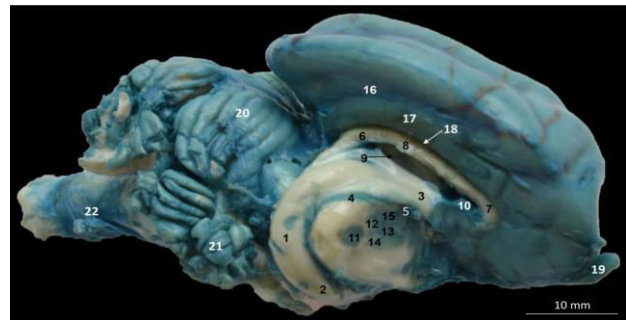

Fig. 9: Mid-sagittal section of the right telencephalic hemisphere of the cat including the hippocampal complex stained with Mulligan staining (Le Masurier). 1: Hippocampus retrocommissuralis, 2: Hippocampal tail or Ammon's horn, 3: Fornix: body, 4: Fimbria of hippocampus, 5: Fornix body, 6: Corpus callosum: splenium, 7: Corpus callosum: genu, 8: Corpus callosum: body, 9: Lateral ventricle (arrow), 10: Septum of the telencephalon, 11: Lateral geniculate nucleus, 12: Rostral thalamic nuclei, 13: Dorsomedial thalamic nucleus, 14: Caudal lateral thalamic nucleus, 15: Habenular nuclei, 16: Splenial sulcus, 17: Cingulate gyrus, 18: Sulcus of corpus callosum (arrow), 19: Olfactory bulb, 20: Cerebellar vermis, 21: Cerebellar hemisphere, and 22: Spinal cord

hyperintense area surrounded by the lateral ventricle. However, the hippocampal complex was fully visualized in a sagittal plane (Fig. 9). At the level of the midbrain, the optic radiation was observed unstained (Figs. 3A-D to 4A-D). In a more caudal section, at the level of the thalamus, the acoustic radiation could be seen in the same way (Figs. 5A-D). These structures could be visualized in MRI, as they were hypointense compared with the grey matter.

The caudate nucleus was stained in a very detailed way close to the thalamus and was visualized in a coronal and parasagittal plane (Figs. 6A-D to 7A-D). It was identified in MRI due to its greater intensity.

The claustrum and the lentiform nuclei (putamen and globus pallidus) were easily identified with the Mulligan technique in stained sections in both the transversal plane (Fig. 5C) and the coronal plane (Fig. 6D). These nuclear structures were not easily visualized in MRI.

The rostral commissure and the corpus callosum appeared unstained in a coronal plane between the two hemispheres (Figs. 6A-D). The corpus callosum was visualized undyed on the stained thalamus and caudate nucleus in a parasagittal and sagittal plane (Figs. 7A-D to 8A-B). These were observed as areas of lower intensity than the grey matter in MRI.

Finally, the course of the ventricular system was identified in a sagittal plane (Figs. 8A-B). In a rostral direction, the ependyma, fourth ventricle, mesencephalic aqueduct, and third ventricle were identified. As it is filled with the cerebrospinal fluid, the ventricular system was seen hyperintense in the T2-weighted sequence.

Discussion

To date, several studies of feline brain anatomy using MRI have been published. Hudson *et al.* (1995) and Mogicato *et al.* (2012) described a feline brain atlas in

which numerous nervous structures were identified in three spatial planes using 1.5 Tesla MR equipment. Przyborowska *et al*. (2017) compared images using two different MRI devices of 0.25 and 3 Tesla. Gray-Edwards *et al*. (2014) obtained MRI using a 3 Tesla MRI apparatus in which T1-weighted and T2-weighted MRI sequences and anatomical sections of the feline brain were used to facilitate interpretation.

The main problem found in the MRI studies of the feline brain is the difficulty of identifying, so many nerve structures and nervous nuclei in such a small brain, and especially when using low-field MRI equipment. Moreover, many structures are identified in these studies without any apparent intensity changes in MRI, which makes their accurate location difficult to achieve.

In this study, we emphasize the value of Mulligan staining as a helpful tool for interpreting MRI obtained from MR equipment used in veterinary centres. The Mulligan staining is a specific histological technique for nervous tissue in which the grey matter absorbs the stain. The intensity of stain varies according to the amount of grey matter existing in the area, and thus, the most stained areas show a bigger impact on nervous centres or nuclei. Moreover, out of the three described techniques, LeMasurier's method facilitates a clearer differentiation between grey and white matter, and thus the visualization of nervous nuclei and centres.

Using stained specimens of most caudal cross sections of the brainstem, we highlight the differentiation of the cerebellar nuclei (emboliform, globose, and fastigial) in MRI. These nuclei were previously identified by Gray-Edwards *et al*. (2014), and Przyborowska *et al*. (2017), but their differentiation in the MRI was barely evident. Clinically, a lesion at the level of the fastigial nucleus produces motor deficits (Zhang *et al*., 2016). Leigh *et al*. (2008) report that cats' anisocoria is the most frequent neurological abnormality related to a lesion at the level of the feline cerebellar nuclei.

The vestibular nuclei located ventral to the cerebellar nuclei were clearly stained and their location is correlated in MRI to hyperintense areas T2-weighted. Both Gray-Edwards *et al*. (2014), and Przyborowska *et al*. (2017) located these nuclei in the thickness of the medulla oblongata, but without evidence of the intensity changes that delimit them in the MRI. Leigh *et al*. (2008) link central vestibular syndrome and loss of physiologic nystagmus to damage at the level of the vestibular nuclei.

In a more rostral section at the midbrain level, staining differentiated the red nucleus within the reticular formation to which it belonged and it was possible to correlate its location correctly as a hyperintense area in T2-weighted images. The red nucleus was not identified in any of the images in the works of Hudson *et al*. (1995), Mogicato *et al*. (2012), Gray-Edwards *et al*. (2014), or Przyborowska *et al*. (2017). This nucleus has been previously mentioned by Leigh *et al*. (2008) but it was not clearly defined in MRI.

Mogicato *et al*. (2012) states that many structures located in the brain stem cannot be identified in MRI due to the similar intensity of nuclei and the surrounding structures. Our study facilitates the identification of the substantia nigra, changes related to Parkinson's disease (Sugiyama *et al*., 2018). The substantia nigra was mentioned by Grey-Edwards *et al*. (2014), and Przyborowska *et al*. (2017), but there were no evident intensity changes in the MRI at this level. Leigh *et al*. (2008) established the relationship between injuries at the level of the substantia nigra with neurological abnormalities (hemiparesis or tetraparesis).

In the telencephalon, the hippocampus is one of the structures that was stained in more detail in the three spatial planes and consequently its location in MRI. The hippocampal nucleus was identified as a hyperintense area in the side wall of the lateral ventricles in the T2-weighted sequence, and due to Mulligan staining, its limits could be defined very accurately. Leigh *et al*. (2008) described a lesion at the level of the limbic system (e.g., amygdala, hippocampus) with behavioural changes and aggression. In the metathalamus, Grey-Edwards *et al*. (2014), and Przyborowska *et al*. (2017) identified the lateral geniculate nucleus. We also identified it at both mesencephalic/diencephalic and thalamic levels with the Mulligan staining and MRI as well. Leigh *et al*. (2008) described lesions at the level of the lateral geniculate body, which produced a decreased menace response with a normal pupillary reflex.

The thalamus contains a large number of nuclei, so it is stained compactly. With Mulligan staining and referring to Nickel *et al*. (1988), the thalamic paraventricular nuclei, the incerta zone and the subthalamic nucleus were identified. In addition, the epithalamic habenular nuclei, as well as the hypothalamic mammillary nuclei, were also identified. Mogicato *et al*. (2012), Grey-Edwards *et al*. (2014), and Przyborowska *et al*. (2017) did not describe any hypothalamic or epithalamic nuclei. Only Hudson *et al*. (1995) identified the lateral nucleus of the thalamus, which is difficult to observe in a very diffuse area. Leigh *et al*. (2008) reflected that a lesion at the level of the thalamic nuclei causes seizures, normal gait with postural reaction deficit, and hypalgesia.

The putamen and pallidum, parts of the lentiform nucleus, appeared stained and were divided by the lamina medullaris lateralis. Pathological alterations at this level have been studied in humans as related conditions such as heart attacks or intracerebral haemorrhages affecting these nuclei with movement disorders (Park, 2016). When stained with Mulligan technique, the claustrum was also clearly identified in our study and T2-weighted as well, but it has not been identified in any of the images in the papers of Hudson *et al*. (1995), Mogicato *et al*. (2012), Gray-Edwards *et al*. (2014) or Przyborowska *et al*. (2017). This is the first time that the claustrum is identified in MRI in cats. Regarding this nucleus, its function is unclear, although it is believed that it could function in maintaining integrated consciousness (Crick and Koch, 2005). Gray-Edwards *et al*. (2014), and Przyborowska *et al*. (2017) identified only the putamen, but not clearly. In our study,

the use of staining allowed us to obtain a clear distinction between both parts of the lentiform nucleus. However, their identification in MRI was difficult because no changes in signal intensity were observed, but correlation with stained sections helped identify their location.

The staining in coronal and parasagittal sections allowed for the correct identification of the caudate nucleus as it stains well and it is located in a hyperintense area in MRI. The papers published by Hudson *et al.* (1995), Mogicato *et al.* (2012), Grey-Edwards *et al.* (2014), and Przyborowska *et al.* (2017) did not describe any hypothalamic or epithalamic nuclei. The function of the caudate nucleus in cats has been studied by Villablanca (2010), who assigned it putative functions such as control of attachment behaviour.

The lateral geniculate body occurs at the level of the metathalamus and Hudson *et al.* (1995), Grey-Edwards *et al.* (2014), and Przyborowska *et al.* (2017) located it, although its presence is not clearly evident. In this study, this structure appeared well delimited by uptake of staining and its localization was possible in MRI as a hyperintense area close to the third ventricle. The correct description of the lateral geniculate nucleus allows advancement in studies related to vision (Onodera and Hicks, 2009; Nakamura, 2018).

The ceruleus nucleus was identified in sagittal sections, rostroventral to the cerebellum. Its identification was provided with Mulligan staining because it was dyed with the three stain techniques and this aided its visualization in MRI. None of the previous atlases of the feline brain (Hudson *et al.*, 1995; Mogicato *et al.*, 2012; Grey-Edwards *et al.*, 2014; Przyborowska *et al.*, 2017) had identified the ceruleus nucleus, so this study is the first to identify it in cats. The ceruleus nucleus is the main noradrenergic nucleus of the brain and plays a primary role in numerous physiological functions such as regulation of excitation and autonomous activity.

In sagittal sections of the brainstem, none of the previously mentioned studies (Mogicato *et al.*, 2012; Grey-Edwards *et al.*, 2014; Przyborowska *et al.*, 2017) identify brain nuclei. Only Hudson *et al.* (1995) located the olivary nucleus. With Mulligan staining, the olivary nucleus and pons nuclei were identified and correlated with MRI. Therefore, this is the first time that the pons nuclei have been visualized in MRI in cats.

This study considers both the anatomical and pathological aspects of nervous structures and nuclei, although many of these conditions have been described only in humans. The present study is proposed as a tool to serve future studies of each brain nucleus and its pathology in cats.

In addition, this work highlights the value of the Mulligan technique in the identification of brain nuclei, as some of these structures have been clearly identified for the first time.

Acknowledgements

Conflict of interest

The authors of this manuscript have no conflict of interest to declare.

References

Barnard, JW; Roberts, JO and Brown, JG (1949). A simple macroscopic staining and mounting procedure for wet sections from cadaver brains. Anat. Rec., 105: 11-17.

Claßen, AC; Kneissl, S; Lang, J; Tichy, A and Pakazdy, A (2016). Magnetic resonance features of the feline hippocampus in epileptic and non-epileptic cats: a blinded, retrospective, multi-observer study. BMC Vet. Res., 12: 165-171.

Crick, FC and Koch, C (2005). What is the function of the claustrum? Philos. Trans. R. Soc. Lond. B Biol. Sci., 360: 1271-1279.

Das, A and Takahashi, E (2018). Characterization of white matter tracts by diffusion MR tractography in cat and ferret that have similar gyral patterns. Cereb. Cortex., 28: 1338-1347.

De Meneses, MS; Montano, JCP; Fuzza, RF and Milano, JB (2004). Comparative analysis of sections of human brain stained by three different techniques. Arq. Neuropsiquiatr., 62: 276-281.

Dos Santos, EC; Da Luz Veronez, DA; De Almeida, DB; Piedade, GS; Oldoni, C; De Meneses, MS and Marques, MS (2019). Morphometric study of the internal globus pallidus using the Robert, Barnard, and Brown staining method. World Neurosurg., 126: e371-e378.

Ghaznawi, R; De Bresser, J; Van der Graaf, Y; Zwartbol, MH; Witkamp, TD; Geerlings, MI; Hendrikse, J and SMART Study Group (2018). Detection and characterization of small infarcts in the caudate nucleus on 7 Tesla MRI: The SMART-MR study. J. Cereb. Blood Flow Metab., 38: 1609-1617.

Gray-Edwards, HL; Salibi, N; Josephson, EM; Hudson, JA; Cox, NR; Randle, AN; McCurdy, VJ; Bradbury, AM; Wilson, DU; Beyers, RJ; Denney, TS and Martin, DR (2014). High resolution MRI anatomy of the cat brain at 3 Tesla. J. Neurosci. Methods. 227: 10-17.

Hespel, AM and Cole, RC (2018). Advances in high-field MRI. Vet. Clin. North Am. Small Anim. Pract., 48: 11-21.

Hudson, LC; Cauzinille, L; Kornegay, JN and Tompkins, MB (1995). Magnetic resonance imaging of the normal feline brain. Vet. Radiol. Ultrasound., 36: 267-275.

Johnson, PJ; Pascalau, R; Luh, WM; Raj, A; Cerda-Gonzalez, S and Barry, EF (2020). Stereotaxic diffusion tensor imaging white matter atlas for the *in vivo* domestic feline brain. Front. Neuroanat., 14: 1-13.

Leigh, EJ; Mackillop, E; Robertson, ID and Hudson, LC (2008). Clinical anatomy of the canine brain using magnetic resonance imaging. Vet. Radiol. Ultrasound., 49: 113-121.

LeMasurier, HE (1935). Simple method of staining macroscopic brain sections. Arq. Neuropsych., 34: 1065-1067.

Mogicato, G; Conchou, F; Layssol-Lamour, C; Raharison, F and Sautet, J (2012). Normal feline brain: clinical anatomy using magnetic resonance imaging. Anat. Histol. Embryol., 41: 87-95.

Mooncey, MS and Sagoo, MG (2014). Comparative staining methods with room temperature plastination (15-18ºC) of brain specimens, using Biodur S10/S3. J. Plast., 26: 21-29.

Müllhaupt, D; Augsburger, H; Schwarz, A; Fischer, G; Kircher, P; Hatt, JM and Ohlerth, S (2015). Magnetic resonance imaging anatomy of the rabbit brain at 3 T. Acta Vet. Scand., 57: 47-55.

Mulligan, JH (1931). A method of staining the brain for macroscopic study. J. Anat., 65: 468-472.

Nakamura, H (2018). Cerebellar projections to the ventral lateral geniculate nucleus and the thalamic reticular nucleus in the cat. J. Neurosci. Res., 96: 63-74.

Nickel, R; Schummer, A and Seiferle, E (1988). *Anatomical treatise of domestic mammals*. Vol. IV, 1st Edn., Casa Editrice Ambrosiana. Milano. PP: 1-439.

Oldoni, C; Luz Veronez, DAD; Piedade, GS; Santos, ECD; Almeida, DB and Meneses, MS (2018). Morphometric analysis of the nucleus accumbens using the Mulligan staining method. World Neurosurg., 118: e223-e228.

Onodera, S and Hicks, TP (2009). A comparative neuroanatomical study of the red nucleus of the cat, macaque and human. PloS One. 4: e6623-e6641.

Park, J (2016). Movement disorders following cerebrovascular lesion in the basal ganglia circuit. J. Mov. Disord., 9: 71-79.

Przyborowska, P; Adamiak, Z; Holak, P and Zhalniarovich, Y (2017). Comparison of feline brain anatomy in 0.25 and 3 Tesla magnetic resonance images. Anat. Histol. Embryol., 46: 178-186.

Sandoval, J (2000). *Veterinary anatomy treatise*. Vol. III: *Head and visceral systems*. 2nd Edn., Leon: Imprenta Sorles. PP: 1-457.

Stolzberg, D; Wong, C; Butler, BE and Lomber, SG (2017). Catlas: An magnetic resonance imaging-based three-dimensional cortical atlas and tissue probability maps for the domestic cat (*Felis catus*). J. Comp. Neurol., 525: 3190-3206.

Sugiyama, A; Sato, N; Kimura, Y; Ota, M; Maekawa, T; Sone, D; Enokizono, M; Murata, M; Matsuda, H and Kuwabara, S (2018). MR findings in the substantia nigra on phase difference enhanced imaging in neuro-degenerative parkinsonism. Parkinsonism Relat Disord., 48: 10-16.

Villablanca, JR (2010). Why do we have a caudate nucleus? Acta Neurobiol. Exp. (Wars)., 70: 95-105.

Zhang, XY; Wang, JJ and Zhu, JN (2016). Cerebellar fastigial nucleus: from anatomic construction to physiological functions. Cerebellum Ataxias., 3: 9-18.